A novel four-legged loaded element thick-screen frequency selective surface with a stable performance

Tang Guang-Ming(唐光明)†, Miao Jun-Gang(苗俊刚), and Dong Jin-Ming(董金明)

School of Electronic and Information Engineering, Beihang University, Beijing 100191, *China*

(Received 9 April 2012; revised manuscript received 30 May 2012)

A thick-screen frequency selective surface (FSS) has not only a broad bandwidth but also the advantages of overcoming the multilayer FSS shortcoming of complex structure and low transmittance of centre frequency due to the cascade of FSSs, and this means it could potentially be applied in a stealth curved streamlined radome. However, there is an unsteadiness of centre frequency in a wide range of incident angles and another unsteadiness of polarization in a big incident angle. In order to solve these problems, in this paper we provide a novel four-legged loaded element thick-screen FSS. The structure is analysed and simulated using the mode matching method and moment method. The centre frequency, the transmittance of centre frequency, and bandwidth of the structure are investigated when some parameters including the polarization at a big incident angle and the incident angles of TE & TM waves are changed. The novel four-legged loaded element thick-screen FSS has better transmission properties with a better steadiness of polarization and incident angle independence. The novel structure of the four-legged loaded element thick-screen FSS provides a valuable reference for their application in a stealth curved streamlined radome.

Keywords: thick-screen frequency selective surfaces (FSS), mode matching method, moment method, incident angles independence, polarization independence

PACS: 84.40.–x **DOI:** 10.1088/1674-1056/21/12/128401

1. Introduction

In the radome designs of aircraft, missiles, satellites, and ships, the frequency selective surface (FSS) with frequency filter characteristics is used to control the transmission of an electromagnetic wave because the FSS can reduce the radar cross section (RCS) of radar antenna systems[1] and ensure the target-weapons have a stealthy performance. However, few publications report on its valuable data because of its important military applications. Now the number of researchers studying FSS are increasing, and a lot of research work has been done and different shapes have been simulated.[2−7] Because the thick-screen frequency selective surface (FSS) has not only a broad bandwidth but also the advantage of overcoming the multilayer FSS shortcomings of a complex structure and low transmittance of centre frequency, owing to the cascade of FSSs, it has a potential application in the stealth curved streamlined radome. In recent years, researchers have paid more and more attention to the thick-screen FSS. So far, there have been few academic articles dealing with this subject because of its military purposes. Björn *et al.*[8] analysed and simulated the transmission performances of circle and hexagon thick-screen FSS structures using the mode matching method. Fang *et al.*[9,10] analysed and simulated a circular aperture thick-screen FSS structure transmission performance with the dielectric using the mode matching method and the moment method. Tang *et al.* analysed and simulated a dielectric-metal-loaded thick-screen FSS having a circular aperture element[11] and a novel Y element thick-screen FSS with a stable performance[12] using the mode matching method and the moment method. In the aforementioned thick-screen FSS, there exists a centre frequency drift in a wide range of incident angles, and the stable performance of polarization in a big incident angle was not investigated. To solve these problems, a novel structure of a four-legged loaded element thick-screen FSS as shown in Fig. 1 is designed in this paper. The novel structure has pass-band properties with a better performance of polarization independence and incident angle independence, and it provides a valuable reference for its application in the stealth curved streamlined radome.

†Corresponding author. E-mail: gmt971@ee.buaa.edu.cn

© 2012 Chinese Physical Society and IOP Publishing Ltd

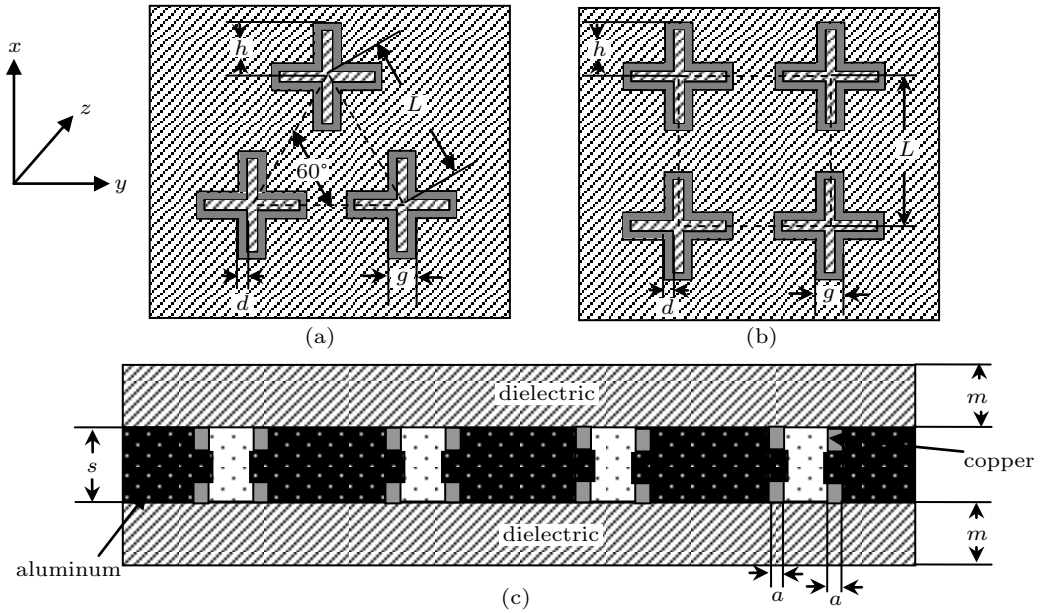


Fig. 1. The novel structure of a four-legged loaded element thick-screen FSS (a) regular triangle arrays (x–y plane), (b) square arrays (x–y plane), (c) square arrays (y–z plane).

2. Model and theoretical analysis

Figure 2 shows an equivalent model of the novel four-legged loaded element thick-screen FSS. There are three waveguide layers (B, C, D) and three dielectric layers (A, F, $J\ldots$) in the model. In Fig. 2, $S^{(0)}$, $S^{(5)}$, $S^{(6)}$ are interfaces between two dielectric layers; $S^{(1)}$ and $S^{(4)}$ are the interfaces respectively between a waveguide layer and a dielectric layer; $S^{(2)}$ and $S^{(3)}$ are the interfaces respectively between two waveguide layers; z_0, z_1, z_2, z_3, z_4, z_5, and z_6 are the coordinates of the interfaces respectively between two layers on the z axis. If the scattering coefficient matrixes in a waveguide layer, a dielectric layer, an interface between two dielectric layers, an interface between two waveguide layers, and an interface between a waveguide layer and a dielectric layer can be computed respectively, and the transmission properties of the novel four-legged loaded element thick-screen FSS can be studied.

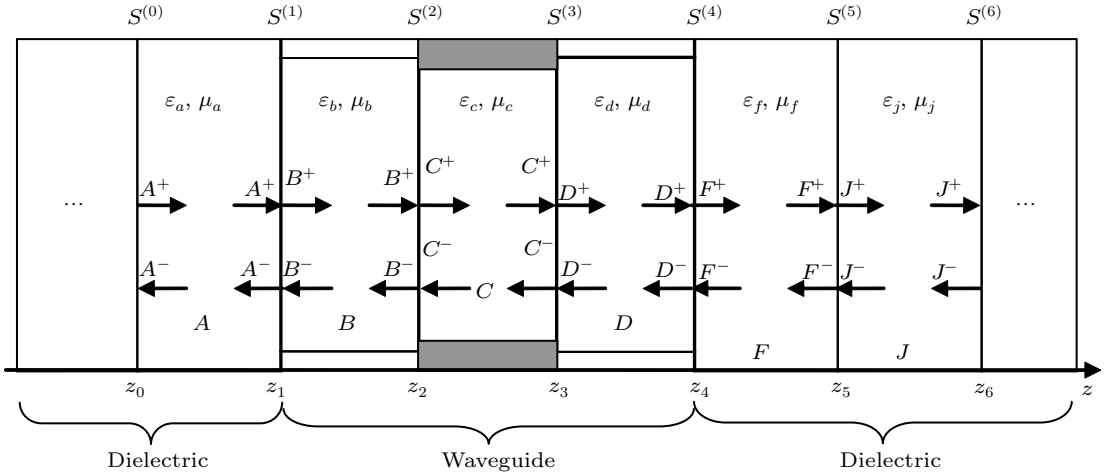


Fig. 2. Equivalent model of the novel four-legged loaded element thick-screen FSS.

2.1. Scattering coefficient matrixes in a waveguide layer

When the electromagnetic wave passes through the B waveguide layer, the following relationships of scattering coefficients exist on each side of the area:

$$\begin{cases} B_{vn}^{+}(z_2) = \boldsymbol{I}\,\mathrm{e}^{\mathrm{i}k_{zn}(z_2-z_1)}B_{vn}^{+}(z_1), \\ B_{vn}^{-}(z_2) = \boldsymbol{I}\,\mathrm{e}^{-\mathrm{i}k_{zn}(z_2-z_1)}B_{vn}^{-}(z_1), \end{cases} \tag{1}$$

which can be represented in the matrix form by

$$\begin{bmatrix}\boldsymbol{B}^-(z_1)\\ \boldsymbol{B}^+(z_2)\end{bmatrix}=\begin{bmatrix}0 & \boldsymbol{E}^b(z_2-z_1)\\ \boldsymbol{E}^b(z_2-z_1) & 0\end{bmatrix}\begin{bmatrix}\boldsymbol{B}^+(z_1)\\ \boldsymbol{B}^-(z_2)\end{bmatrix}, \quad (2)$$

where

$$\boldsymbol{E}^b_{vn,v'n'}(z)=\mathrm{e}^{\mathrm{i}k_{zn}z}\delta_{vv'}\delta_{nn'},$$
$$(\delta_{vv'}\delta_{nn'}=\int \boldsymbol{E}^b_{Tvn}(x,y)\cdot\boldsymbol{E}^{b^*}_{Tv'n'}(x,y)\mathrm{d}x\mathrm{d}y).$$

Similarly, when the electromagnetic wave passes through waveguide layers C and D, the scattering coefficient matrixes on each side of the area are written respectively as

$$\begin{bmatrix}\boldsymbol{C}^-(z_2)\\ \boldsymbol{C}^+(z_3)\end{bmatrix}=\begin{bmatrix}0 & \boldsymbol{E}^c(z_3-z_2)\\ \boldsymbol{E}^c(z_3-z_2) & 0\end{bmatrix}\begin{bmatrix}\boldsymbol{C}^+(z_2)\\ \boldsymbol{C}^-(z_3)\end{bmatrix}, \quad (3)$$

$$\begin{bmatrix}\boldsymbol{D}^-(z_3)\\ \boldsymbol{D}^+(z_4)\end{bmatrix}=\begin{bmatrix}0 & \boldsymbol{E}^d(z_4-z_3)\\ \boldsymbol{E}^d(z_4-z_3) & 0\end{bmatrix}\begin{bmatrix}\boldsymbol{D}^+(z_3)\\ \boldsymbol{D}^-(z_4)\end{bmatrix}, \quad (4)$$

where

$$\boldsymbol{E}^c_{vn,v'n'}(z)=\mathrm{e}^{\mathrm{i}k_{zn}z}\delta_{vv'}\delta_{nn'},$$
$$\Big(\delta_{vv'}\delta_{nn'}=\int \boldsymbol{E}^c_{Tvn}(x,y)\cdot\boldsymbol{E}^{c^*}_{Tv'n'}(x,y)\mathrm{d}x\mathrm{d}y\Big),$$
$$\boldsymbol{E}^d_{vn,v'n'}(z)=\mathrm{e}^{\mathrm{i}k_{zn}z}\delta_{vv'}\delta_{nn'},$$
$$\Big(\delta_{vv'}\delta_{nn'}=\int \boldsymbol{E}^d_{Tvn}(x,y)\cdot\boldsymbol{E}^{d^*}_{Tv'n'}(x,y)\mathrm{d}x\mathrm{d}y\Big).$$

2.2. Scattering coefficient matrixes in a dielectric layer

When the electromagnetic wave passes through dielectric layer A, the following relationships of scattering coefficients exist on each side of the area:

$$\begin{cases}A^+_{mn}(z_1)=\boldsymbol{I}\,\mathrm{e}^{\mathrm{i}\gamma_{mn}(z_1-z_0)}A^+_{mn}(z_0),\\ A^-_{mn}(z_1)=\boldsymbol{I}\,\mathrm{e}^{-\mathrm{i}\gamma_{mn}(z_1-z_0)}A^-_{mn}(z_0),\end{cases} \quad (5)$$

which can be represented in the matrix form as

$$\begin{bmatrix}\boldsymbol{A}^-(z_0)\\ \boldsymbol{A}^+(z_1)\end{bmatrix}=\begin{bmatrix}0 & \boldsymbol{E}^a(z_1-z_0)\\ \boldsymbol{E}^a(z_1-z_0) & 0\end{bmatrix}\begin{bmatrix}\boldsymbol{A}^+(z_0)\\ \boldsymbol{A}^-(z_1)\end{bmatrix}, \quad (6)$$

where

$$\boldsymbol{E}^a_{mn,m'n'}(z)=\mathrm{e}^{\mathrm{i}\gamma_{mn}z}\delta_{mm'}\delta_{nn'},$$
$$\Big(\delta_{mm'}\delta_{nn'}=\int \boldsymbol{E}^a_{Tmn}(x,y)\cdot\boldsymbol{E}^{a*}_{Tm'n'}(x,y)\mathrm{d}x\mathrm{d}y\Big).$$

Similarly, when the electromagnetic wave passes through waveguide layers F, J, etc., the scattering coefficients matrixes on each side of the area will be obtained.

2.3. Scattering coefficient matrixes at the interface between two dielectric layers

In order to compute the scattering coefficient matrix between dielectric layer F and dielectric layer J, firstly, the fields in the layers are expanded using the Floquet theorem as follows:

$$\boldsymbol{E}^f_T(x,y,z)=\sum_{lmn}\big(f^+_{lmn}\,\mathrm{e}^{\mathrm{i}\gamma^f_{mn}z}+f^-_{lmn}\,\mathrm{e}^{-\mathrm{i}\gamma^f_{mn}z}\big)\boldsymbol{R}^f_{Tlmn}(x,y),\quad (z<z_5), \quad (7)$$

$$\boldsymbol{H}^f_T(x,y,z)=\sum_{lmn}\big(f^+_{lmn}\,\mathrm{e}^{\mathrm{i}\gamma^f_{mn}z}-f^-_{lmn}\,\mathrm{e}^{-\mathrm{i}\gamma^f_{mn}z}\big)\boldsymbol{T}^f_{Tlmn}(x,y),\quad (z<z_5), \quad (8)$$

$$\boldsymbol{E}^j_T(x,y,z)=\sum_{lmn}\big(j^+_{lmn}\,\mathrm{e}^{\mathrm{i}\gamma^j_{mn}z}+j^-_{lmn}\,\mathrm{e}^{-\mathrm{i}\gamma^j_{mn}z}\big)\boldsymbol{R}^j_{Tlmn}(x,y),\quad (z>z_5), \quad (9)$$

$$\boldsymbol{H}^j_T(x,y,z)=\sum_{lmn}\big(j^+_{lmn}\,\mathrm{e}^{\mathrm{i}\gamma^j_{mn}z}-j^-_{lmn}\,\mathrm{e}^{-\mathrm{i}\gamma^j_{mn}z}\big)\boldsymbol{T}^j_{Tlmn}(x,y),\quad (z>z_5). \quad (10)$$

Then, let $z=z_5$ at the interface between two layers. So the boundary conditions ensure that the magnetic fields and the tangential electric fields are continuous on the entire interface K of the two layers. The boundary conditions are defined as

$$\boldsymbol{E}^f_T(x,y,z_5)=\boldsymbol{E}^j_T(x,y,z_5),\ (x,y\in K), \quad (11)$$

$$\boldsymbol{H}^f_T(x,y,z_5)=\boldsymbol{H}^j_T(x,y,z_5),\ (x,y\in K). \quad (12)$$

Because

$$F^\pm_{lmn}(z)=f^\pm_{lmn}\,\mathrm{e}^{\pm\mathrm{i}\gamma^f_{mn}z},\quad J^\pm_{lmn}(z)=j^\pm_{lmn}\,\mathrm{e}^{\pm\mathrm{i}\gamma^j_{mn}z},$$

we obtain

$$\sum_{lmn}(F^+_{lmn}(z_5)+F^-_{lmn}(z_5))\boldsymbol{R}^f_{Tlmn}(x,y)$$
$$=\sum_{lmn}(J^+_{lmn}(z_5)+J^-_{lmn}(z_5))\boldsymbol{R}^j_{Tlmn}(x,y),\quad (x,y\in K), \quad (13)$$

$$\sum_{lmn}(F^+_{lmn}(z_5)-F^-_{lmn}(z_5))\boldsymbol{T}^f_{Tlmn}(x,y)$$
$$=\sum_{lmn}(J^+_{lmn}(z_5)-J^-_{lmn}(z_5))\boldsymbol{T}^j_{Tlmn}(x,y),\quad (x,y\in K). \quad (14)$$

The inner products are taken between Eq. (13) and $\boldsymbol{T}^{f*}_{Tl'm'n'}$, and between Eq. (14) and $\boldsymbol{R}^{j*}_{Tl'm'n'}$. Finally, the scattering coefficient matrix between dielectric layer F and dielectric layer J is obtained as fol-

lows:

$$\begin{bmatrix} \boldsymbol{F}^-(z_5) \\ \boldsymbol{J}^+(z_5) \end{bmatrix} = \begin{bmatrix} S_{11}^{(5)} & S_{12}^{(5)} \\ S_{21}^{(5)} & S_{22}^{(5)} \end{bmatrix} \begin{bmatrix} \boldsymbol{F}^+(z_5) \\ \boldsymbol{J}^-(z_5) \end{bmatrix}, \tag{15}$$

where

$$S_{11}^{(5)} = -(\boldsymbol{T}^f + \boldsymbol{W}^t \boldsymbol{T}^{j^*-1} \boldsymbol{W}^*)^{-1}(\boldsymbol{T}^f - \boldsymbol{W}^t \boldsymbol{T}^{j^*-1} \boldsymbol{W}^*),$$
$$S_{12}^{(5)} = 2(\boldsymbol{T}^f + \boldsymbol{W}^t \boldsymbol{T}^{j^*-1} \boldsymbol{W}^*)^{-1} \boldsymbol{W}^t,$$
$$S_{21}^{(5)} = 2(\boldsymbol{T}^{j^*} + \boldsymbol{W}^* \boldsymbol{T}^{f-1} \boldsymbol{W}^t)^{-1} \boldsymbol{W}^*,$$
$$S_{22}^{(5)} = (\boldsymbol{T}^{j^*} + \boldsymbol{W}^* \boldsymbol{T}^{f-1} \boldsymbol{W}^t)^{-1}(\boldsymbol{T}^{j^*} - \boldsymbol{W}^* \boldsymbol{T}^{f-1} \boldsymbol{W}^t),$$

including

$$T^f_{lmn,l'm'n'} = \frac{Y^{f*}_{lmn}}{\eta_0} \delta_{ll'} \delta_{mm'} \delta_{nn'},$$
$$T^j_{lmn,l'm'n'} = \frac{Y^{j^*}_{lmn}}{\eta_0} \delta_{ll'} \delta_{mm'} \delta_{nn'},$$
$$W_{lmn,l'm'n'} = \frac{Y^{f^*}_{lmn}}{\eta_0} \delta_{ll'} \delta_{mm'} \delta_{nn'},$$

($\delta_{ll'}\delta_{mm'}\delta_{nn'} = \int \boldsymbol{R}^f_{Tlmn}(x,y) \cdot \boldsymbol{R}^{f^*}_{Tlmn}(x,y) \mathrm{d}x \mathrm{d}y$, Y is an admittance matrix).

Similarly, in the presence of many dielectric layers, the scattering coefficient matrix between two dielectric layers will be obtained.

2.4. Scattering coefficient matrixes on an interface between a dielectric layer and a waveguide layer

To compute the scattering coefficient matrixes on an interface between a dielectric layer and a waveguide layer, firstly, the fields in dielectric layer A are expanded using the Floquet theorem as follows:

$$\boldsymbol{E}^a_T(x,y,z) = \sum_{lmn} \left(a^+_{lmn} \mathrm{e}^{\mathrm{i}\gamma^a_{mn} z} + a^-_{lmn} \mathrm{e}^{-\mathrm{i}\gamma^a_{mn} z}\right) \boldsymbol{R}^a_{Tlmn}(x,y), \quad (z < z_1), \tag{16}$$

$$\boldsymbol{H}^a_T(x,y,z) = \sum_{lmn} \left(a^+_{lmn} \mathrm{e}^{\mathrm{i}\gamma^a_{mn} z} - a^-_{lmn} \mathrm{e}^{-\mathrm{i}\gamma^a_{mn} z}\right) \boldsymbol{T}^a_{Tlmn}(x,y), \quad (z < z_1), \tag{17}$$

while the fields in waveguide B are expanded using waveguide modes as

$$\boldsymbol{E}^b_T(x,y,z) = \sum_{vn} \left(b^+_{vn} \mathrm{e}^{\mathrm{i}k^b_{zn} z} + b^-_{vn} \mathrm{e}^{-\mathrm{i}k^b_{zn} z}\right) \boldsymbol{E}^b_{Tvn}(x,y), \quad (z > z_1), \tag{18}$$

$$\boldsymbol{H}^b_T(x,y,z) = \sum_{vn} \left(b^+_{vn} \mathrm{e}^{\mathrm{i}k^b_{zn} z} - b^-_{vn} \mathrm{e}^{-\mathrm{i}k^b_{zn} z}\right) \boldsymbol{H}^b_{Tvn}(x,y), \quad (z > z_1). \tag{19}$$

Then, let $z = z_1$ at the interface between two layers. So the boundary conditions ensure that the magnetic fields are continuous on the aperture Ω, while the tangential electric fields are continuous on the entire interface I between the two layers. The boundary conditions are defined as

$$\boldsymbol{E}^a_T(x,y,z_1) = \begin{cases} \boldsymbol{E}^b_T(x,y,z_1), & (x,y \in \Omega), \\ 0, & (x,y \in I \backslash \Omega), \end{cases} \tag{20}$$

$$\boldsymbol{H}^a_T(x,y,z_1) = \boldsymbol{H}^b_T(x,y,z_1)(x,y \in \Omega). \tag{21}$$

Because

$$A^\pm_{lmn}(z) = a^\pm_{lmn} \mathrm{e}^{\pm \mathrm{i}\gamma^a_{mn} z}, \quad B^\pm_{vn}(z) = b^\pm_{vn} \mathrm{e}^{\pm \mathrm{i}k^b_{zn} z},$$

we obtain

$$\sum_{lmn} (A^+_{lmn}(z_1) + A^-_{lmn}(z_1)) \boldsymbol{R}^a_{Tlmn}(x,y) = \begin{cases} \sum\limits_{vn} (B^+_{vn}(z_1) + B^-_{vn}(z_1)) \boldsymbol{E}^b_{Tvn}(x,y), & (x,y \in \Omega), \\ 0, & (x,y \in I \backslash \Omega), \end{cases} \tag{22}$$

$$\sum_{lmn} (A^+_{lmn}(z_1) - A^-_{lmn}(z_1)) \boldsymbol{T}^a_{Tlmn}(x,y) = \sum_{vn} (B^+_{vn}(z_1) - B^-_{vn}(z_1)) \boldsymbol{H}^b_{Tvn}(x,y), \quad (x,y \in \Omega). \tag{23}$$

The inner products are taken between Eq. (32) and $\boldsymbol{T}^{a*}_{Tl'm'n'}$, and between Eq. (33) and $\boldsymbol{E}^{b^*}_{Tv'n'}$. Finally, the scattering coefficient matrix between dielectric layer F and dielectric layer J is obtained as follows:

$$\begin{bmatrix} \boldsymbol{A}^-(z_1) \\ \boldsymbol{B}^+(z_1) \end{bmatrix} = \begin{bmatrix} S_{11}^{(1)} & S_{12}^{(1)} \\ S_{21}^{(1)} & S_{22}^{(1)} \end{bmatrix} \begin{bmatrix} \boldsymbol{A}^+(z_1) \\ \boldsymbol{B}^-(z_1) \end{bmatrix}, \tag{24}$$

where

$$S_{11}^{(1)} = -(\boldsymbol{P} + \boldsymbol{G}^t \boldsymbol{Q}^{*-1} \boldsymbol{G}^*)^{-1}(\boldsymbol{P} - \boldsymbol{G}^t \boldsymbol{Q}^{*-1} \boldsymbol{G}^*), \quad S_{12}^{(1)} = 2(\boldsymbol{P} + \boldsymbol{G}^t \boldsymbol{Q}^{*-1} \boldsymbol{G}^*)^{-1} \boldsymbol{G}^t,$$
$$S_{21}^{(1)} = 2(\boldsymbol{Q}^* + \boldsymbol{G}^* \boldsymbol{P}^{-1} \boldsymbol{G}^t)^{-1} \boldsymbol{G}^*, \quad S_{22}^{(1)} = (\boldsymbol{Q}^* + \boldsymbol{G}^* \boldsymbol{P}^{-1} \boldsymbol{G}^t)^{-1}(\boldsymbol{Q}^* - \boldsymbol{G}^* \boldsymbol{P}^{-1} \boldsymbol{G}^t),$$

including

$$P_{lmn,l'm'n'} = \frac{Y^{a^*}_{vn}}{\eta_0}\delta_{ll'}\delta_{mm'}\delta_{nn'}, \quad G_{vn,l'm'n'} = \frac{Y^{a^*}_{l'm'n'}}{\eta_0}\int (\boldsymbol{E}^b_{Tvn}\cdot\boldsymbol{R}^{a^*}_{Tl'm'n'})\mathrm{d}S, \quad Q_{vn,v'n'} = \frac{Y^{b^*}_{vn}}{\eta_0}\delta_{vv'}\delta_{nn'},$$

(Y is an admittance matrix, $\delta_{ll'}\delta_{mm'}\delta_{nn'} = \int \boldsymbol{R}^a_{Tlmn}(x,y)\cdot\boldsymbol{R}^{a^*}_{Tl'm'n'}(x,y)\mathrm{d}x\mathrm{d}y$, $\delta_{vv'}\delta_{nn'} = \int \boldsymbol{E}^b_{Tvn}(x,y)\cdot\boldsymbol{E}^{b^*}_{Tv'n'}(x,y)\mathrm{d}x\mathrm{d}y$).

Similarly, the scattering coefficient matrix between dielectric layer F and waveguide layer D will be obtained as follows:

$$\begin{bmatrix}\boldsymbol{D}^-(z_4)\\ \boldsymbol{F}^+(z_4)\end{bmatrix} = \begin{bmatrix}S^{(4)}_{11} & S^{(4)}_{12}\\ S^{(4)}_{21} & S^{(4)}_{22}\end{bmatrix}\begin{bmatrix}\boldsymbol{D}^+(z_4)\\ \boldsymbol{F}^-(z_4)\end{bmatrix}, \tag{25}$$

where

$$S^{(4)}_{11} = S^{(1)}_{22}, \quad S^{(4)}_{12} = S^{(1)}_{21}, \quad S^{(4)}_{21} = S^{(1)}_{12}, \quad S^{(4)}_{22} = S^{(1)}_{11}.$$

2.5. Scattering coefficient matrixes on an interface between two waveguide layers

In order to compute the scattering coefficient matrix between waveguide layer B and waveguide layer C, firstly, the fields in the layers are expanded using waveguide modes as follows:

$$\boldsymbol{E}^b_T(x,y,z) = \sum_{vn}(b^+_{vn}\,\mathrm{e}^{\mathrm{i}k^b_{zn}z} + b^-_{vn}\,\mathrm{e}^{-\mathrm{i}k^b_{zn}z})\boldsymbol{E}^b_{Tvn}(x,y), \quad (z<z_2), \tag{26}$$

$$\boldsymbol{H}^b_T(x,y,z) = \sum_{vn}(b^+_{vn}\,\mathrm{e}^{\mathrm{i}k^b_{zn}z} - b^-_{vn}\,\mathrm{e}^{-\mathrm{i}k^b_{zn}z})\boldsymbol{H}^b_{Tvn}(x,y), \quad (z<z_2), \tag{27}$$

$$\boldsymbol{E}^c_T(x,y,z) = \sum_{vn}(c^+_{vn}\,\mathrm{e}^{\mathrm{i}k^c_{zn}z} + c^-_{vn}\,\mathrm{e}^{-\mathrm{i}k^c_{zn}z})\boldsymbol{E}^c_{Tvn}(x,y), \quad (z>z_2), \tag{28}$$

$$\boldsymbol{H}^c_T(x,y,z) = \sum_{vn}(c^+_{vn}\,\mathrm{e}^{\mathrm{i}k^c_{zn}z} - c^-_{vn}\,\mathrm{e}^{-\mathrm{i}k^c_{zn}z})\boldsymbol{H}^c_{Tvn}(x,y), \quad (z>z_2). \tag{29}$$

Then, let $z=z_2$ at the interface between two layers. So the boundary conditions ensure that the tangential magnetic fields are continuous on the junction N, while the tangential electric fields are continuous on the entire interface M between the two layers. The boundary conditions are defined as

$$\boldsymbol{E}^b_T(x,y,z_2) = \begin{cases}\boldsymbol{E}^c_T(x,y,z_2), & (x,y\in N),\\ 0, & (x,y\in M\backslash N),\end{cases} \tag{30}$$

$$\boldsymbol{H}^b_T(x,y,z_2) = \boldsymbol{H}^c_T, \ (x,y,z_2)(x,y\in N). \tag{31}$$

Because

$$B^\pm_{vn}(z) = b^\pm_{vn}\,\mathrm{e}^{\pm\mathrm{i}k^b_{zn}z}, \quad C^\pm_{vn}(z) = c^\pm_{vn}\,\mathrm{e}^{\pm\mathrm{i}k^c_{zn}z},$$

we obtain

$$\sum_{vn}(B^+_{vn}(z_2)+B^-_{vn}(z_2))\boldsymbol{E}^b_{Tvn}(x,y) = \begin{cases}\sum\limits_{vn}(C^+_{vn}(z_2)+C^-_{vn}(z_2))\boldsymbol{E}^c_{Tvn}(x,y), & (x,y\in N),\\ 0, & (x,y\in M\backslash N),\end{cases} \tag{32}$$

$$\sum_{vn}(B^+_{vn}(z_2)-B^-_{vn}(z_2))\boldsymbol{H}^b_{Tvn}(x,y) = \sum_{vn}(C^+_{vn}(z_2)-C^-_{vn}(z_2))\boldsymbol{H}^c_{Tvn}(x,y), \quad (x,y\in N). \tag{33}$$

The inner products are taken between Eq. (32) and $\boldsymbol{H}^{b^*}_{Tv'n'}$, and between Eq. (33) and $\boldsymbol{E}^{c^*}_{Tv'n'}$. Finally, the scattering coefficient matrix between waveguide layer B and waveguide layer C is obtained as follows:

$$\begin{bmatrix}\boldsymbol{B}^-(z_2)\\ \boldsymbol{C}^+(z_2)\end{bmatrix} = \begin{bmatrix}S^{(2)}_{11} & S^{(2)}_{12}\\ S^{(2)}_{21} & S^{(2)}_{22}\end{bmatrix}\begin{bmatrix}\boldsymbol{B}^+(z_2)\\ \boldsymbol{C}^-(z_2)\end{bmatrix}, \tag{34}$$

where

$$\begin{aligned}
S^{(2)}_{11} &= -(\boldsymbol{U}^b + \boldsymbol{V}^t\boldsymbol{U}^{c^*-1}\boldsymbol{V}^*)^{-1}(\boldsymbol{U}^b - \boldsymbol{V}^t\boldsymbol{U}^{c^*-1}\boldsymbol{V}^*),\\
S^{(2)}_{12} &= 2(\boldsymbol{U}^b + \boldsymbol{V}^t\boldsymbol{U}^{c^*-1}\boldsymbol{V}^*)^{-1}\boldsymbol{V}^t,\\
S^{(2)}_{21} &= 2(\boldsymbol{U}^{c^*} + \boldsymbol{V}^*\boldsymbol{U}^{b-1}\boldsymbol{V}^t)^{-1}\boldsymbol{V}^*,\\
S^{(2)}_{22} &= (\boldsymbol{U}^{c^*} + \boldsymbol{V}^*\boldsymbol{U}^{b-1}\boldsymbol{V}^t)^{-1}(\boldsymbol{U}^{c^*} - \boldsymbol{V}^*\boldsymbol{U}^{b-1}\boldsymbol{V}^t),
\end{aligned}$$

including

$$U^b_{vn,v'n'} = \frac{Y^{b^*}_{vn}}{\eta_0}\delta_{vv'}\delta_{nn'},$$

$$U^c_{vn,v'n'} = \frac{Y^{c^*}_{vn}}{\eta_0}\delta_{vv'}\delta_{nn'},$$

$$V_{vn,v'n'} = \frac{Y^{b^*}_{v'n'}}{\eta_0}\int_\Omega (\boldsymbol{E}^c_{Tvn}\cdot\boldsymbol{R}^{b^*}_{Tv'n'})\mathrm{d}S,$$

(Y is an admittance matrix, $\delta_{vv'}\delta_{nn'} = \int \boldsymbol{E}^c_{Tvn}(x,y)\cdot \boldsymbol{E}^{c^*}_{Tv'n'}(x,y)\mathrm{d}x\mathrm{d}y$).

Similarly, the scattering coefficient matrix between waveguide layer C and waveguide layer D will be obtained as follows:

$$\begin{bmatrix}\boldsymbol{C}^-(z_3)\\ \boldsymbol{D}^+(z_3)\end{bmatrix} = \begin{bmatrix}S^{(3)}_{11} & S^{(3)}_{12}\\ S^{(3)}_{21} & S^{(3)}_{22}\end{bmatrix}\begin{bmatrix}\boldsymbol{C}^+(z_3)\\ \boldsymbol{D}^-(z_3)\end{bmatrix}, \quad (35)$$

where

$$S^{(3)}_{11} = S^{(2)}_{22},\ S^{(3)}_{12} = S^{(2)}_{21},\ S^{(3)}_{21} = S^{(2)}_{12},\ S^{(3)}_{22} = S^{(2)}_{11}.$$

After the scattering coefficient matrixes in the layers and their interfaces are computed, the scattering coefficients matrix of the equivalent model of the novel four-legged loaded element thick-screen FSS will be obtained according to the cascade theory. The transmission characteristics of the novel thick-screen FSS will be analysed through solving the matrix of the equivalent model.

In the above discussion, $\boldsymbol{A}^\pm$, $\boldsymbol{B}^\pm$, $\boldsymbol{C}^\pm$, $\boldsymbol{D}^\pm$, $\boldsymbol{F}^\pm$, and $\boldsymbol{J}^\pm$ are the unknown coefficient matrixes. $\boldsymbol{R}_{Tlmn}$ and $\boldsymbol{T}_{Tlmn}$ are the coefficients of reflection and transmission, respectively, and they are in the vector forms of the Floquet wave; $\boldsymbol{R}^*_{Tl'm'n'}$ and $\boldsymbol{T}^*_{Tl'm'n'}$ are their conjugate complex numbers; $\boldsymbol{R}$ and $\boldsymbol{T}$ are in the short forms. a, b, c, and d are superscripts of various layers. If subscript $l = 1$, there is the TE-Floquet mode; if $l = 2$, there is the TM-Floquet mode. If $m = n = 0$, there is a dominant mode of Floquet; if $m \neq 0$ or $n \neq 0$, there is a higher order mode of Floquet. $\boldsymbol{E}_{Tvn}$ and $\boldsymbol{H}_{Tvn}$ are the electric fields and magnetic fields, respectively; and they are in the vector forms of waveguide modes; $\boldsymbol{E}^*_{Tvn}$ and $\boldsymbol{H}^*_{Tvn}$ are their conjugate complex numbers; $\boldsymbol{E}$ and $\boldsymbol{H}$ are in their short forms. If subscript $v = 0$, there is the polarized wave of TEM; if $v = 1$, there is a polarized wave of TE; if $v = 2$, there is the polarized wave of TM. $n = 1, 2, 3, \ldots, +\infty$. The k is the propagation constant of an incident plane wave, γ is the propagation constant of the Floquet wave, and η_0 is the wave impedance in free space.

3. Numerical demonstrations

In order to study the transmission performance of the novel four-legged loaded element thick-screen FSS, the structure is designed as shown in Fig. 1, where $L = 12.88$ mm, $h = 6.25$ mm, $g = 1.25$ mm, $d = 0.38$ mm, $m = 1.00$ mm, $s = 1.5$ mm, $a \to 0$.

3.1. Angle independence of the novel element FSS in the incident plane wave of TE

In the incident plane wave of TE, let $\theta = 0°$, $30°$, $60°$, respectively. Figures 3 and 4 show the simulation curves. Table 1 shows calculation data.

For the case of regular triangle arrays, when θ varies from $0°$ to $30°$, the centre frequency f_0 drifts from 0.01 GHz upward, the bandwidth W at -3 dB reduces by 0.15 GHz, the transmittance T of the centre frequency increases by 0.07 dB; when θ varies from $0°$ to $60°$, the centre frequency f_0 also drifts 0.01 GHz upward, the bandwidth W at -3 dB reduces by 0.60 GHz, and the transmittance T of centre frequency reduces by 0.13 dB.

For the case of square arrays, when θ varies from $0°$ to $30°$, the centre frequency f_0 does not drift, the bandwidth W at -3 dB reduces by 0.15 GHz, the transmittance T of centre frequency does not change; when θ varies from $0°$ to $60°$, the centre frequency f_0 does not drift either, the bandwidth W at -3 dB reduces by 0.55 GHz, and the transmittance T of the centre frequency reduces by 0.52 dB.

Therefore, when the incident plane wave of TE is at various angles, regular triangle arrays and square arrays of the novel element have the same tendencies: the centre frequency changes a little bit with the increase of the incident angles; there is a better angle independence; the bandwidth and transmittance of the centre frequency will decrease with the increase of the incident angle and there is a better transmittance of centre frequency in the two arrays.

The physical mechanism of this phenomenon is as follows. The insertion phase delay is short in the novel four-legged loaded element thick-screen FSS, and the interval of elements in the arrays is small, so that the grating lobe will be produced in a long time; a plate element is placed in an aperture element, so that the distance between two conductors is reduced and the capacitance is increased, thus a strong resonance can be produced at a lower frequency and there is a small mismatch loss; the problem of cross polarization can be solved by symmetrically loading; the coupling between two layers can reach a maximum through appropriately adjusting the positions of the mix elements in combination with the plate and aperture elements, so there is an incident angle independence and a small offset of the centre frequency.

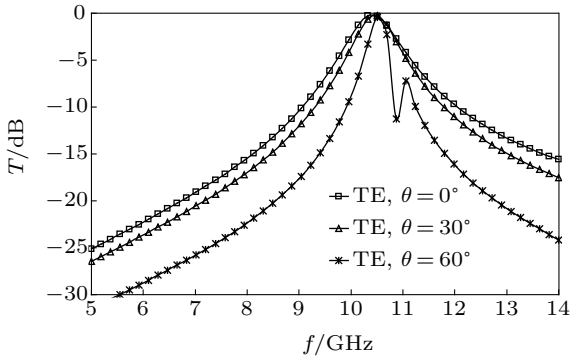


Fig. 3. Angle independences of the novel element FSS in the incident plane wave of TE at three different incident angles for the case of regular triangle arrays.

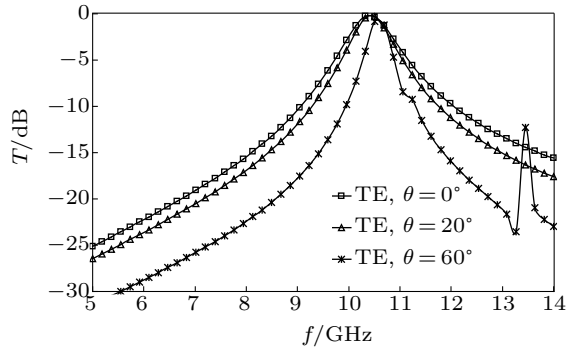


Fig. 4. Angle independences of the novel element FSS in the incident plane wave of TE at three different incident angles for the case of square arrays.

Table 1. Transmission properties of the novel element FSS in various arrays (TE).

Arrays	$\theta/(^\circ)$	f_0/GHz	W/GHz	T/dB
Regular triangle	0	10.50	0.96	−0.30
	30	10.51	0.81	−0.23
	60	10.51	0.36	−0.43
Square	0	10.51	0.96	−0.29
	30	10.51	0.81	−0.29
	60	10.51	0.41	−0.81

3.2. Angle independence of the novel element FSS in the incident plane wave of TM

In the incident plane wave of TM, let $\theta = 0^\circ$, 30°, 60°, respectively. Figures 5 and 6 show the simulation curves. Table 2 shows the calculation results.

For the case of regular triangle arrays, when θ varies from 0° to 30°, the centre frequency f_0 does not drift, the bandwidth W at -3 dB increases by 0.04 GHz, the transmittance T of the centre frequency increases by 0.01 dB; when θ varies from 0° to 60°, the centre frequency f_0 drifts 0.10 GHz upward, the bandwidth W at -3 dB increases by 0.82 GHz, and the transmittance T of the centre frequency is reduced by 0.09 dB.

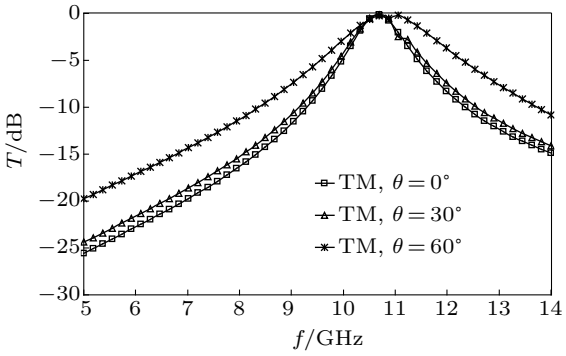


Fig. 5. Angle independences of the novel element FSS in the incident plane wave of TM at three different incident angles for the case of regular triangle arrays.

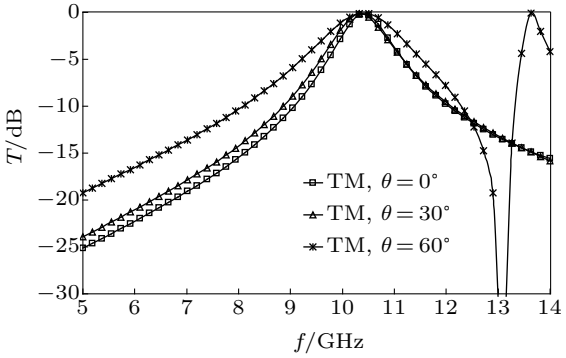


Fig. 6. Angle independences of the novel element FSS in the incident plane wave of TM at three different incident angles for the case of square arrays.

Table 2. Transmission properties of the novel element FSS in various arrays (TM).

Arrays	$\theta/(^\circ)$	f_0/GHz	W/GHz	T/dB
Regular triangle	0	10.69	0.99	−0.14
	30	10.69	1.03	−0.13
	60	10.79	1.81	−0.23
Square	0	10.32	0.97	−0.28
	30	10.32	1.07	−0.13
	60	10.32	1.59	−0.11

For the case of square arrays, when θ varies from 0° to 30°, the centre frequency f_0 does not drift, the bandwidth W at -3 dB increases by 0.10 GHz, the transmittance T of centre frequency increases by 0.15 dB; when θ varies from 0° to 60°, the centre frequency f_0 does not drift either, the bandwidth W at -3 dB increases by 0.62 GHz, and the transmittance T of the centre frequency increases by 0.17 dB.

Therefore, when the incident plane wave of TM is at various incident angles, the tendency of regular triangle arrays is as follows. i) The centre frequency and the bandwidth increase a little with the increase of incident angle. ii) The transmittance of the centre frequency will be changed with a tiny fluctuation; the tendency of square arrays is that the bandwidth and the transmittance of the centre frequency increase a little with the increase of incident angle. There is a better steadinesses of polarization and incident angle independence in the two arrays. The physical mechanism of this phenomenon is similar to that shown in Subsection 3.1.

4. Conclusion

The key factors of application in stealth curved streamlined radomes are polarization independence and incident angle independence. So in this paper, the novel structure of a four-legged loaded element thick-screen FSS is designed. The structure is analysed and simulated using the mode matching method and moment method. The results show that there are better transmission performances in the cases of regular triangle arrays and square arrays. When θ varies from 0° to 60°, there is a small offset of the centre frequency ranging from 0.01 GHz to 0.10 GHz. When the polarization changes from TE to TM at $\theta = 60^\circ$, there are two small offsets of the centre frequency which are 0.19 GHz and 0.10 GHz in the cases of the regular triangle and square arrays, respectively. The novel structure of the four-legged loaded element thick-screen FSS has passband properties with better performances of polarization independence and incident angle independence, and it provides a valuable reference for its application in stealth curved streamlined radomes.

Acknowledgement

The authors would like to thank Sun Jing-Rui, Li Yong-Jia and Zhang Cui-Cui for their helpful discussion.

References

[1] Ben Munk 2000 *Frequency Selective Surfaces Theory and Design* (New York: Wiley)

[2] Sun L K, Cheng H F, Zhou Y J and Wang J 2012 *Chin. Phys.* B **21** 055201

[3] Jia H Y, Feng X G and Sheng C 2012 *Chin. Phys.* B **21** 054102

[4] Zhou H, Qu S B, Peng W D, Lin B Q, Wang J F, Ma H, Zhang J Q, Bai P, Wang X H and Xu Z 2012 *Chin. Phys.* B **21** 054101

[5] Zhou H, Qu S B, Peng W D, Wang J F, Ma H, Zhang J Q, Bai P and Xu Z 2012 *Chin. Phys.* B **21** 030301

[6] Wang L J, Sun J B and Cheng G 2009 *Chin. Phys.* B **18** 1598

[7] Jia H Y, Gao J S and Feng X G 2009 *Chin. Phys.* B **18** 1227

[8] Björn W, Sören P and Anders K. 2000 *Journal of Electromagnetic Waves and Applications* **14** 1303

[9] Fang C Y, Zhang S R, Lu J, Wang J B and Sun L C 2010 *Optics and Precision Engineering* **18** 1278 (in Chinese)

[10] Fang C Y, Zhang S R, Lu J, Wang J B and Sun L C 2010 *Acta Phys. Sin.* **59** 5023 (in Chinese)

[11] Tang G M, Miao J G and Dong J M 2012 *Acta Phys. Sin.* **61** 068402 (in Chinese)

[12] Tang G M, Miao J G, Dong J M and Hu X Q 2012 *Acta Phys. Sin.* **61** 118401 (in Chinese)